S-Palmitoylation of the sodium channel Nav1.6 regulates its activity and neuronal excitability

Received for publication, December 23, 2019, and in revised form, March 10, 2020 Published, Papers in Press, March 11, 2020, DOI 10.1074/jbc.RA119.012423

Yanling Pan[‡], Yucheng Xiao[§], Zifan Pei[¶], and Theodore R. Cummins[‡§¶1]

From the [‡]Program in Medical Neuroscience, Paul and Carole Stark Neurosciences Research Institute and the [¶]Department of Pharmacology and Toxicology, Indiana University School of Medicine, Indianapolis, Indiana 46202 and the [§]Department of Biology, School of Science, Indiana University–Purdue University Indianapolis, Indianapolis, Indiana 46202

Edited by Mike Shipston

S-Palmitoylation is a reversible post-translational lipid modification that dynamically regulates protein functions. Voltage-gated sodium channels are subjected to *S*-palmitoylation and exhibit altered functions in different *S*-palmitoylation states. Our aim was to investigate whether and how *S*-palmitoylation regulates Nav1.6 channel function and to identify *S*-palmitoylation sites that can potentially be pharmacologically targeted. Acyl-biotin exchange assay showed that Nav1.6 is modified by *S*-palmitoylation in the mouse brain and in a Nav1.6 stable HEK 293 cell line. Using whole-cell voltage clamp, we discovered that enhancing *S*-palmitoylation with palmitic acid increases Nav1.6 current, whereas blocking *S*-palmitoylation with 2-bromopalmitate reduces Nav1.6 current and shifts the steady-state inactivation in the hyperpolarizing direction. Three *S*-palmitoylation sites (Cys^{1169}, Cys^{1170}, and Cys^{1978}) were identified. These sites differentially modulate distinct Nav1.6 properties. Interestingly, Cys^{1978} is exclusive to Nav1.6 among all Nav isoforms and is evolutionally conserved in Nav1.6 among most species. Cys^{1978} *S*-palmitoylation regulates current amplitude uniquely in Nav1.6. Furthermore, we showed that eliminating *S*-palmitoylation at specific sites alters Nav1.6-mediated excitability in dorsal root ganglion neurons. Therefore, our study reveals *S*-palmitoylation as a potential isoform-specific mechanism to modulate Nav activity and neuronal excitability in physiological and diseased conditions.

Excitability of a neuron is determined by the composition, distribution, and properties of ion channels in its plasma membrane. It can be profoundly changed by slight alteration in the biophysics of a channel. The voltage-gated sodium channel (Nav)[2] family plays crucial roles in the initiation and propagation of action potentials. The nine Nav isoforms (Nav1.1–Nav1.9) have distinct biophysical properties and differential cellular and subcellular distribution (1). They are responsible for the electrical signal transduction in a wide range of physiological processes. Abnormal or dysregulated Nav activity can lead to varied diseased conditions including epilepsy, pain, autism, cardiac arrhythmia, and skeletal muscle disorders. Therefore, Navs have long been therapeutically desirable targets in the drug discovery industry. However, the high sequence and structural conservation shared among the Navs have posed a significant challenge to the development of isoform-specific therapeutics and modulators with minimum side effects.

Navs consist of four domains (DI–DIV), with each containing six transmembrane segments (S1–S6) (Fig. 1). S1–S4 comprise the voltage sensors, whereas the S5 and S6 regions combine to form the sodium conducting pore. These regions are critical for normal voltage sensing and sodium ion selectivity. They are highly conserved among Nav isoforms. The relatively less conserved extracellular loops are frequent binding sites for peptidic gating modifier toxins like conotoxins, protoxins, and huwentoxins (2, 3). These sites present some degree of isoform specificity and thus have attracted tremendous pharmacological interest over the past two decades (1, 4). The intracellular loops and cytosolic N- and C-terminal domains are heavily involved in protein–protein interactions and are subject to extensive post-translational modifications (5). Importantly, they contain highly variable regions. Therefore, understanding the important roles of the Nav intracellular loops and their post-translational modifications may identify new strategies to help target Navs with improved specificity.

In recent years, *S*-palmitoylation has emerged as an important mechanism that regulates protein functions. It is a reversible post-translational modification that covalently attaches palmitate, a 16-carbon saturated fatty acid, to cysteine thiols in a protein via thioester bonds. Because *S*-palmitoylation alters protein hydrophobicity, it has the potential to impose significant structural and thus functional changes on proteins. It can regulate membrane association, trafficking, conformation, and protein–protein interactions of a diverse range of proteins (6–8). It also plays crucial roles in ion channel regulation (5, 9–14). It has been shown that *S*-palmitoylation substantially modulates cardiac excitability by modifying the cardiac sodium channel Nav1.5 (9) and that manipulating the *S*-palmitoylation status of Nav1.2 can alter its voltage dependence and toxin sensitivity (10). Moreover, the enzyme families involved in

This work was supported by NINDS, National Institutes of Health Grant NS053422 (to T. R. C.). The authors declare that they have no conflicts of interest with the contents of this article. The content is solely the responsibility of the authors and does not necessarily represent the official views of the National Institutes of Health.

This article contains Fig. S1.

[1] To whom correspondence should be addressed: Dept. of Biology, School of Science, IUPUI, Indianapolis, IN 46202. Tel.: 317-278-9342; Fax: 317-274-2846; E-mail: trcummin@iu.edu.

[2] The abbreviations used are: Nav, voltage-gated sodium channel; PAT, palmitoyl-acyl transferase; DRG, dorsal root ganglion; ABE, acyl-biotin exchange; TTX, tetrodotoxin; TTXr, TTX-resistant; 2BP, 2-bromopalmitate; PA, palmitic acid; CTD, C-terminal domain; CNS, central nervous system; EGFP, enhanced GFP; ANOVA, analysis of variance.

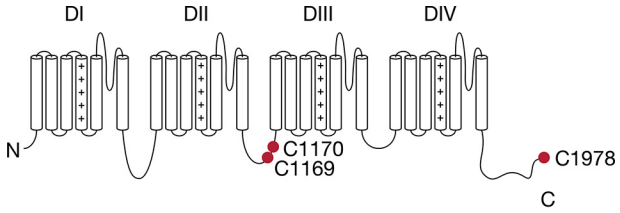

Figure 1. Topology of a voltage-gated sodium channel showing positions of the three predicted *S*-palmitoylation sites in Nav1.6.

S-palmitoylation and depalmitoylation, palmitoyl-acyl transferase (PAT) and acyl protein thioesterases, display differential but overlapping specificity for substrate proteins (15–20). This evidence suggests that *S*-palmitoylation may be well-fitted to convey isoform-specific modulation of Navs.

In our study, we show that Nav1.6 is chemically modified and functionally regulated by *S*-palmitoylation. We identify two *S*-palmitoylation sites (Cys^{1169} and Cys^{1170}) in the second intracellular loop (loop 2) that are responsible for modulating the voltage dependence of inactivation and an Nav1.6-exclusive site (Cys^{1978}) at the C terminus, the *S*-palmitoylation of which enhances Nav1.6 current. It is important to note that the current amplitude of Nav1.2, which lacks the C-terminal cysteine, is not subject to *S*-palmitoylation enhancement, whereas the introduction of an exogenous cysteine at this site recapitulates the response of Nav1.6. Additionally, we find that eliminating *S*-palmitoylation at Cys^{1169}, Cys^{1170}, and Cys^{1978} reduces Nav1.6-mediated excitability of dorsal root ganglion (DRG) neurons. Therefore, our data reveal *S*-palmitoylation as a novel mechanism that regulates Nav1.6 activity and neuronal excitability.

Results

Nav1.6 is post-translationally modified by S-palmitoylation

Some Nav isoforms are modified by *S*-palmitoylation. The cardiac sodium channel Nav1.5 was shown to be biochemically modified and functionally regulated by *S*-palmitoylation (9). Additionally, functional properties and toxin sensitivity of Nav1.2 are altered by manipulating the *S*-palmitoylation status of the channel with pharmacological treatment (10). However, it is unclear whether Nav1.6 is modified by *S*-palmitoylation. To test this, we performed acyl-biotin exchange (ABE) assay on proteins extracted from the mouse cerebellum because of its enriched expression of Nav1.6 as well as the HEK 293 cell line stably expressing Nav1.6. Fig. 2*A* shows that Nav1.6 is *S*-palmitoylated in the mouse brain and the Nav1.6 cell line.

S-Palmitoylation modulates Nav1.6 current amplitude and voltage dependence of inactivation

Next we explored how *S*-palmitoylation regulates Nav1.6 channel function (Table 1). Because of the difficulty of achieving satisfactory level of Nav1.6 expression in the HEK 293 cell line with heterologous cDNA transfection, we used the ND7/23 cells, a hybrid cell line of mouse neuroblastoma fused with rat dorsal root ganglia neurons (21), as our expression system for Nav1.6 transient transfection and voltage clamp recordings. Because ND7/23 cells do not express tetrodotoxin-resistant (TTXr) sodium channels (22), the Nav1.6 construct was rendered resistant to TTX (Nav1.6r) by a Y371S substitution (23), and 500 nM TTX was added to the extracellular solution for patch clamp recordings to isolate Nav1.6r currents. To manipulate the *S*-palmitoylation status of the Nav1.6r channel, we incubated the transfected cells for overnight with either 25 μM 2-bromopalmitate (2BP) to block *S*-palmitoylation or 10 μM palmitic acid (PA) to enhance *S*-palmitoylation. These concentrations of 2BP and PA were determined previously for optimal *S*-palmitoylation blockage and enhancement (9), and it has been verified that these treatments manipulate protein *S*-palmitoylation status in our expression system as expected (Fig. 3*H*).

Fig. 2*B* shows the representative traces of Nav1.6r currents from each treatment group. We found that blocking *S*-palmitoylation with 2BP reduces Nav1.6 current by 67% (2BP: -26.30 ± 3.29 pA/pF *versus* DMSO: -80.16 ± 8.30 pA/pF; $p < 0.0001$), whereas increasing *S*-palmitoylation substrate availability with PA treatment enhances Nav1.6 current by 78% (PA: -142.4 ± 17.27 pA/pF; $p = 0.0021$ PA *versus* DMSO) (Fig. 2*C*). Notably, the current density in the PA group is more than 5-fold of the 2BP group. To eliminate the possibility that these bidirectional effects were mediated by different mechanisms, transfected cells were simultaneously treated with 25 μM 2BP and 10 μM PA. The current density of the co-treated cells (-32.12 ± 7.43 pA/pF) is similar to that of the 2BP group ($p = 0.3365$ 2BP + PA *versus* 2BP) (Table 1), suggesting that the current density effects produced by the separate 2BP and PA treatments are very likely mediated by *S*-palmitoylation. These data support the contention that 2BP effectively blocks *S*-palmitoylation in our expression system, although excessive *S*-palmitoylation substrate was provided to bias the palmitoylation–depalmitoylation equilibrium.

We next examined whether *S*-palmitoylation affects the voltage dependence of Nav1.6. We observed that blocking *S*-palmitoylation with 2BP causes an 8-mV hyperpolarizing shift of steady-state inactivation (2BP: $V_{½} = -72.34 \pm 0.28$ mV *versus* DMSO: $V_{½} = -64.46 \pm 0.21$ mV; $p < 0.0001$), similar to the modulation observed with Nav1.2 (10) and Nav1.5 (9). Moreover, blocking *S*-palmitoylation resulted in a slower recovery from inactivation (Fig. 2*E*, *2BP*: $\tau = 13.18 \pm 1.28$ ms *versus* DMSO: $\tau = 9.84 \pm 0.76$ ms; $p = 0.0246$). On the other hand, increasing *S*-palmitoylation substrate availability with PA treatment does not alter Nav1.6 voltage dependence of activation, steady-state inactivation, or recovery from inactivation. The lack of modulation by PA treatment may be due to saturation of *S*-palmitoylation at the site(s) regulating voltage dependence of Nav1.6 in our expression system. Thus, providing excessive *S*-palmitoylation substrate does not achieve appreciable alteration in channel function. In contrast, *S*-palmitoylation at the site(s) that regulate Nav1.6 current amplitude (Fig. 2, *B* and *C*) are likely not saturated, demonstrated by the opposing effects of 2BP and PA treatments. Therefore, our data suggest that *S*-palmitoylation regulates distinct functional properties of Nav1.6, potentially by modifying different *S*-palmitoylation sites in the channel.

S-Palmitoylation of Nav1.6 at Cys^{1169} and Cys^{1170} regulates voltage dependence of steady-state inactivation

To identify *S*-palmitoylation sites responsible for the observed functional modulations in Nav1.6, we used CSS-Palm (24) for

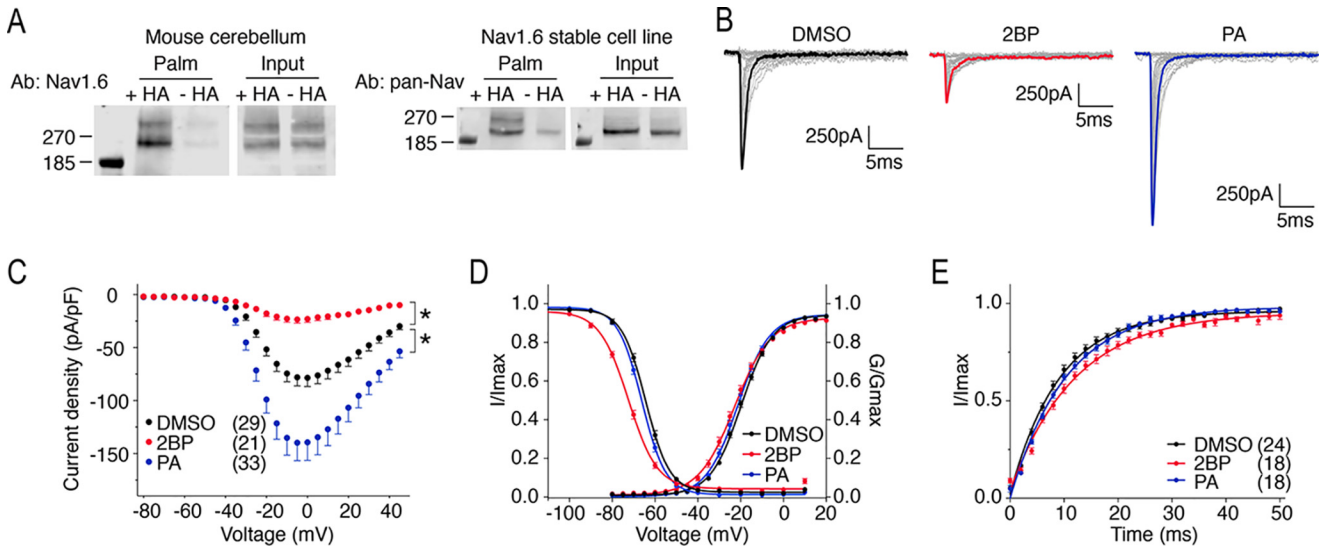

Figure 2. *S*-Palmitoylation post-translationally modifies Nav1.6 and functionally regulates Nav1.6 current amplitude and voltage dependence of inactivation. *A*, acyl-biotin exchange assay on mouse cerebellum probed with Nav1.6 antibody (*left panel*) and on HEK cell line stably expressing Nav1.6 probed with pan-Nav antibody (*right panel*). *B–E*, voltage-clamp experiments on ND7/23 cells transiently transfected with TTXr–Nav1.6. Transfected cells were treated with DMSO as solvent control, 2BP to block *S*-palmitoylation, and PA to enhance *S*-palmitoylation 24 h before recording. *B*, representative current traces from each treatment group elicited with the activation protocol. Maximum current traces are indicated with *black*, *red*, and *blue*, respectively. *C*, current density–voltage plot. *, $p < 0.05$ compared with DMSO in two-way ANOVA. *D*, steady-state inactivation and activation curves fitted with Boltzmann functions. *E*, recovery from inactivation with recovery time duration from 0 to 50 ms. The data are presented as means ± S.E. The values and statistical significance are reported in Table 1.

Table 1
Biophysical properties of WT and mutant Nav1.6 and Nav1.2 channel

			Inactivation			Activation			Recovery	
	Max I density	*n*	V_{half}	*K*	*n*	V_{half}	*K*	*n*	τ	*n*
	pA/pF		*mV*			*mV*			*ms*	
Nav1.6-WT										
DMSO	−80.17 ± 8.30	29	−64.46 ± 0.21	5.32 ± 0.138	30	−19.7 ± 0.18	7.045 ± 0.13	28	9.842 ± 0.76	24
2BP	−26.30 ± 3.29	21[a]	−72.34 ± 0.28[a]	6.51 ± 0.243[a]	28	−22.48 ± 0.84[b]	7.802 ± 0.16[c]	22	13.18 ± 1.28[b]	18
PA	−142.8 ± 17.24	33[c, d]	−66.12 ± 0.18	5.162 ± 0.08	33	−21.32 ± 0.2	6.92 ± 0.203[e]	33	10.54 ± 0.45	18
2BP + PA	−32.12 ± 7.43	12[c]								
Nav1.6-CCAA										
DMSO	−94.17 ± 17.23	19	−75.50 ± 0.39[f]	7.205 ± 0.19[g]	26	−22.59 ± 0.93[f]	7.93 ± 0.37[g]	18	10.70 ± 0.38	21
2BP	−52.09 ± 5.11	19[b]	−80.48 ± 0.30[c]	6.824 ± 0.22	22	−25.88 ± 0.83[b]	8.10 ± 0.22	17	12.69 ± 0.69[b]	10
PA	−163.3 ± 24.30	18[b, d]	−73.57 ± 0.32[e]	6.767 ± 0.19	21	−22.48 ± 0.98[j]	7.85 ± 0.18	17	10.45 ± 0.31[h]	19
Nav1.6-C1978A										
DMSO	−113.2 ± 13.68	35	−63.79 ± 0.23	5.446 ± 0.08	34	−19.81 ± 0.76	7.228 ± 0.12	35	10.32 ± 0.31	21
2BP	−74.20 ± 12.70	27[i]	−73.59 ± 1.39[a]	7.107 ± 0.14[a]	22	−21.66 ± 0.99	7.76 ± 0.57	17	12.82 ± 0.57[c]	26
PA	−120.5 ± 16.18	27[j]	−63.62 ± 0.29[d]	5.369 ± 0.11[d]	27	−17.95 ± 0.82[h]	7.203 ± 0.14	28	10.48 ± 0.55[h]	23
Nav1.6-CCCAAA										
DMSO	−115.8 ± 15.01	25	−72.91 ± 0.44[g]	7.143 ± 0.18[g]	21	−18.75 ± 0.2	8.58 ± 0.165[g]	23	12.68 ± 0.54	19
2BP	−83.50 ± 9.69	22[k]	−79.56 ± 0.35[l]	7.196 ± 0.18	21	−21.61 ± 0.2[c]	8.491 ± 0.10	16	14.36 ± 0.68	15
PA	−117.5 ± 12.84	26[m]	−75.05 ± 0.37[j]	7.779 ± 0.29	22	−18.05 ± 0.5[h]	9.671 ± 1.18	19	12.73 ± 0.55	17
DRG-Nav1.6										
WT	−2006 ± 294.9	20	−78.30 ± 1.27	5.936 ± 0.197	20	−34.57 ± 2.16	7.113 ± 0.625	18	11.35 ± 1.17	20
CCCAAA	−1026 ± 124.7	29[c]	−85.17 ± 2.24[b]	9.952 ± 0.659[a]	25	−31.63 ± 1.37	8.721 ± 0.403[b]	27	9.355 ± 0.56	26
Nav1.2-WT										
DMSO	−648.7 ± 69.50	30	−57.79 ± 0.18	4.868 ± 0.06	26	−15.01 ± 0.2	6.743 ± 0.24	26	7.968 ± 0.38	22
2BP	−397.3 ± 47.31	28[c]	−61.95 ± 0.21[a]	5.474 ± 0.15[l]	24	−14.59 ± 0.1	7.479 ± 0.16[b]	27	10.41 ± 0.80[c]	21
PA	−641.2 ± 92.95	23[j]	−54.01 ± 0.10[a, e]	4.705 ± 0.10[d]	21	−12.43 ± 0.2[b]	6.704 ± 0.23[j]	21	7.437 ± 0.39[h]	20
Nav1.2 K2005C										
DMSO	−562.1 ± 62.34	28	−57.20 ± 0.18	4.88 ± 0.088	30	−14.82 ± 0.2	6.608 ± 0.21	27	8.702 ± 0.53	22
2BP	−416.5 ± 52.65	29[n]	−62.91 ± 0.25[a]	5.33 ± 0.078[l]	29	−17.29 ± 0.2	7.212 ± 0.17	25	11 ± 0.579[c]	26
PA	−837.1 ± 134.8	31[j, o]	−55.57 ± 0.21[d]	4.849 ± 0.08[e]	27	−16.13 ± 0.2	6.028 ± 0.30[h]	27	7.384 ± 0.34[d]	23

[a] $p < 0.0001$ compared with DMSO of the same DNA. [b] $p <$ compared with DMSO of the same DNA. [c] $p < 0.01$ compared with DMSO of the same DNA. [d] $p < 0.0001$ PA compared with 2BP of the same DNA. [e] $p < 0.001$, PA compared with 2BP of the same DNA. [f] $p < 0.01$, mutant compared with WT. [g] $p < 0.05$, mutant compared with WT. [h] $p < 0.01$, PA compared with 2BP of the same DNA. [i] $p = .054$. [j] $p < 0.05$, PA compared with 2BP of the same DNA. [k] $p = .115$. [l] $p < 0.001$ compared with DMSO of the same DNA. [m] $p = .091$. [n] $p = .162$ compared with DMSO of the same DNA. [o] $p = .074$ compared with 2BP of the same DNA.

potential site prediction. In Nav1.6, two cysteines (Cys^{1169} and Cys^{1170}) located near the AnkG-binding motif (residues 1094–1102) in loop 2 were predicted to be *S*-palmitoylated (Fig. 1). These two cysteines are highly conserved among human Nav isoforms (Fig. 3*A*), yet their functions vary: depalmitoylation of the first cysteine in Nav1.2 (Cys^{1182}) was reported to enhance Nav1.2 inactivation (10), whereas the homologous cysteine in Nav1.5 (Cys^{1178}) was not involved in such modulation (9). This

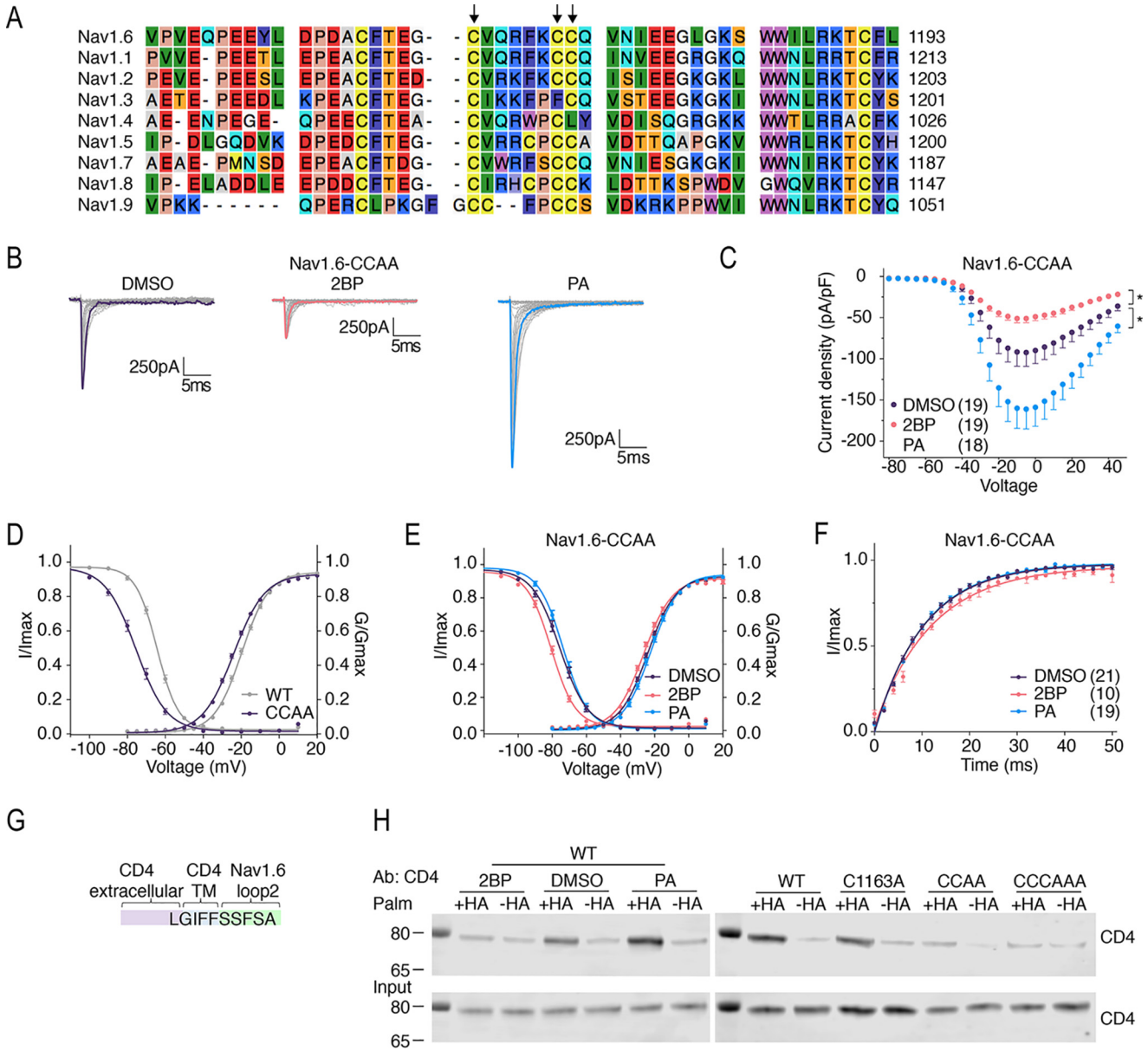

Figure 3. *S*-Palmitoylation of Cys^{1169} and Cys^{1170} regulates Nav1.6 voltage dependence of inactivation, but not Nav1.6 current amplitude. *A*, a segment of amino acid alignment of the Nav family. *Arrows* indicate Cys^{1163}, Cys^{1169}, and Cys^{1170} in Nav1.6. *B*, representative current traces elicited from Nav1.6–CCAA with different treatments. *C*, current density–voltage plot. *, $p < 0.05$ compared with DMSO in two-way ANOVA. *D* and *E*, steady-state inactivation and activation curves of Nav1.6–WT and Nav1.6–CCAA fitted with Boltzmann functions. *F*, recovery from inactivation with recovery time duration from 0 to 50 ms. The data are presented as means ± S.E. The values and statistical significance are reported in Table 1. *G*, schematic illustration of the CD4–Nav1.6–loop 2 fusion protein showing the last five amino acids of the CD4 transmembrane segment and the first five amino acids of the Nav1.6–loop 2. *H*, acyl-biotin exchange assays on fusion protein-transfected HEK cells probed with CD4 antibody. *Left panels*, WT fusion protein transfected cells treated with DMSO, 2BP, and PA. *Right panels*, WT, C1163A, CCAA, and CCCAAA fusion proteins.

indicates potential isoform-specific functionality of *S*-palmitoylation. We were interested to test whether *S*-palmitoylation of the homologous cysteines in Nav1.6 regulates channel function and how it might differ from Nav1.2 and Nav1.5. For this purpose, we eliminated *S*-palmitoylation at Cys^{1169} and Cys^{1170} by mutating both to nonpalmitoylatable alanines (Nav1.6–CCAA) and evaluated the functional consequences. Fig. 3*B* shows the representative traces of TTXr Nav1.6–CCAA current from each treatment group. Compared with Nav1.6–WT, Nav1.6–CCAA displays an 11-mV hyperpolarizing shift in voltage dependence of steady-state inactivation ($V_{½}$ = −75.5 ± 0.39 mV; $p < 0.0001$) (Fig. 3*D*). This replicates the voltage dependence modulation observed in Nav1.6–WT with *S*-palmitoylation blockage, suggesting that *S*-palmitoylation at these two cysteines is critical for voltage dependence regulation of Nav1.6. However, the Nav1.6–CCAA channel does not completely lose its sensitivity to 2BP treatment and has a minor hyperpolarizing shift in steady-state inactivation ($V_{½}$ = −80.48 ± 0.30 mV; $p = 0.0046$) (Fig. 3*E*). Consistent with the WT channel, increasing *S*-palmitoylation substrate availability with PA treatment does not alter the voltage dependence of activation, steady-state inactivation (Fig. 3*E*), or recovery from inactivation (Fig. 3*F*) of Nav1.6–CCAA, whereas blocking *S*-palmitoylation with 2BP treatment results in slower recovery

from inactivation (2BP: τ = 12.69 ± 0.69 ms; DMSO: τ = 10.70 ± 0.38 ms; p = 0.0114). Interestingly, Nav1.6–CCAA exhibits the same bidirectional current density response to 2BP and PA treatments as the WT channel (Fig. 3*C*), indicating that Cys^{1169} and Cys^{1170} do not contribute to regulating Nav1.6 current amplitude.

To biochemically confirm *S*-palmitoylation occurs at Cys^{1169} and Cys^{1170}, we designed a CD4–Nav1.6–loop 2 fusion protein for use in the ABE assay because of the low expression level of Nav1.6 in the heterologous expression system (Fig. 3*G*). Using this construct, we observed that the *S*-palmitoylation signal of the CD4–loop 2 fusion protein can be enhanced by PA treatment and reduced by 2BP treatment in our expression system (Fig. 3*H*), and the signals are within the linear range of detection (Fig. S1*A*). Moreover, eliminating *S*-palmitoylation at the cysteines corresponding to Cys^{1169} and Cys^{1170} in Nav1.6 (loop 2–CCAA) greatly reduces the *S*-palmitoylation signal compared with the WT fusion protein, suggesting that Cys^{1169} and Cys^{1170} are major *S*-palmitoylation sites in Nav1.6–loop 2. However, *S*-palmitoylation is not completely abolished in loop 2–CCAA. This may indicate additional *S*-palmitoylation sites in the fusion protein. Intriguingly, Cys^{1163}, a cysteine near the double cysteines 1169 and 1170 (Fig. 1), becomes a predicted *S*-palmitoylation site in CSS-Palm in both Nav1.6–CCAA and loop 2–CCAA, whereas it is not a predicted site in the WT proteins. This suggests the possibility of unmasking and favoring *S*-palmitoylation at noncanonical residues when primary *S*-palmitoylation sites are eliminated in a protein. Indeed, the ABE assay showed that loop 2–C1163A displays similar *S*-palmitoylation signal as loop 2–WT, suggesting that Cys^{1163} is not a major *S*-palmitoylation site, although it might become one when neighboring *S*-palmitoylation sites are removed (*e.g.* loop 2–CCAA). This may also explain the extra hyperpolarizing shift of steady-state inactivation observed in the Nav1.6–CCAA channel with 2BP treatment (Fig. 3*E*), even though the CCAA mutant itself could account for a comparable inactivation shift in the WT channel with 2BP treatment.

Nav1.6 Cys^{1978} confers the regulation of current amplitude in response to S-palmitoylation enhancement

Because *S*-palmitoylation at Cys^{1169} and Cys^{1170} is only involved in regulating Nav1.6 voltage dependence, we set out to identify the *S*-palmitoylation site(s) responsible for Nav1.6 current amplitude regulation. Cys^{1978} is another predicted *S*-palmitoylation site. It is the last residue of Nav1.6, located at the very end of the cytoplasmic C-terminal domain (CTD) (Fig. 1). This site is of tremendous interest, because it is exclusive to Nav1.6 and is not found in any other isoform in the Nav family (Fig. 4*A*). More importantly, Cys^{1978} is evolutionally conserved among Nav1.6 for most species (Fig. S1*B*). These observations indicate that Cys^{1978} may convey crucial isoform-specific function for Nav1.6. Moreover, there is evidence that *S*-palmitoylation in the CTD of ion channels plays a role in surface targeting (13, 25, 26). Therefore, we hypothesized that Nav1.6–Cys^{1978} *S*-palmitoylation regulates Nav1.6 surface expression and thus produces the opposite current density effects observed with 2BP and PA treatments. To test this hypothesis, we eliminated *S*-palmitoylation at Cys^{1978} in Nav1.6 and examined the functional properties of this mutant channel. Fig. 4*B* shows the representative traces of TTXr Nav1.6–C1978A current from each treatment group. We found that increasing *S*-palmitoylation substrate availability with PA treatment no longer increases Nav1.6 current (PA: −120.50 ± 16.18 pA/pF, *versus* DMSO: 113.2 ± 13.68 pA/pF; p = 0.8123) (Fig. 4*C*). However, blocking *S*-palmitoylation with 2BP still slightly decreases Nav1.6–C1978A current (−74.20 ± 12.70 pA/pF), although the reduction does not reach statistical significance (p = 0.0544) (Fig. 4*C*). We speculated that this decrease of Nav1.6–C1978A current by 2BP treatment may be accounted for by secondary *S*-palmitoylation site(s) or other unknown mechanisms, similar to the additional hyperpolarization of steady-state inactivation in Nav1.6–CCAA observed with 2BP treatment. Importantly, Nav1.6–C1978A demonstrates the same voltage dependence response to 2BP and PA treatments as Nav1.6–WT (Fig. 4, *D* and *E*), suggesting that *S*-palmitoylation at Cys^{1978} does not regulate voltage dependence of the channel. Using the same fusion protein strategy as in Fig. 3*G*, we confirmed Cys^{1978} as a major *S*-palmitoylation site in the Nav1.6–CTD (Fig. 4, *G* and *H*). It is noteworthy that there is no functional interaction or competition between *S*-palmitoylation at Cys^{1169}, Cys^{1170} and that at Cys^{1978}, because the triple cysteine mutant (Nav1.6–CCCAAA) with all three cysteines mutated to alanines replicates the voltage-dependent response of Nav1.6–CCAA and the current density response of Nav1.6–C1978A (Fig. 4, *I–K*). Together, our data demonstrate that *S*-palmitoylation at different residues of Nav1.6 differentially regulates distinct channel functions.

Nav1.2 current is not increased by S-palmitoylation enhancement, but an exogenous cysteine renders it sensitive to the regulation

Because the C-terminal cysteine (Cys^{1978}) is exclusive to Nav1.6, we predicted that other Nav isoforms would lack similar current amplitude regulation by *S*-palmitoylation. To address this question, we evaluated how *S*-palmitoylation affects the functional properties of Nav1.2. Nav1.2 has a high degree of sequence homology and a similar expression pattern in the central nervous system as Nav1.6. However, it has a lysine (Lys^{2005}) at the homologous position to Nav1.6–Cys^{1978}. Fig. 5*A* shows the representative traces of Nav1.2–WT currents. We found that increasing *S*-palmitoylation substrate availability with PA treatment does not increase Nav1.2 current density (PA: −641.2 ± 92.95 pA/pF *versus* DMSO: −648.7 ± 69.50 pA/pF; p = 0.8517) (Fig. 5*B*), although blocking *S*-palmitoylation with 2BP decreases Nav1.2 current (−397.3 ± 47.31 pA/pF; p = 0.0074) (Fig. 5*B*). This resembles the pattern of current density response to 2BP and PA treatments observed in the Nav1.6–C1978A channel. This suggested that Navs lacking *S*-palmitoylation at the C terminus are not subject to current amplitude increased by *S*-palmitoylation. On the contrary, the voltage dependence of steady-state inactivation of Nav1.2 is altered by its *S*-palmitoylation states (Fig. 5*C*): blocking *S*-palmitoylation with 2BP causes a 4-mV hyperpolarizing shift (2BP: $V_{½}$ = −61.95 ± 0.21 mV *versus* DMSO: $V_{½}$ = −57.79 ± 0.18 mV; $p < 0.0001$), whereas increasing *S*-palmitoylation substrate availability results in a 4-mV depolarizing shift

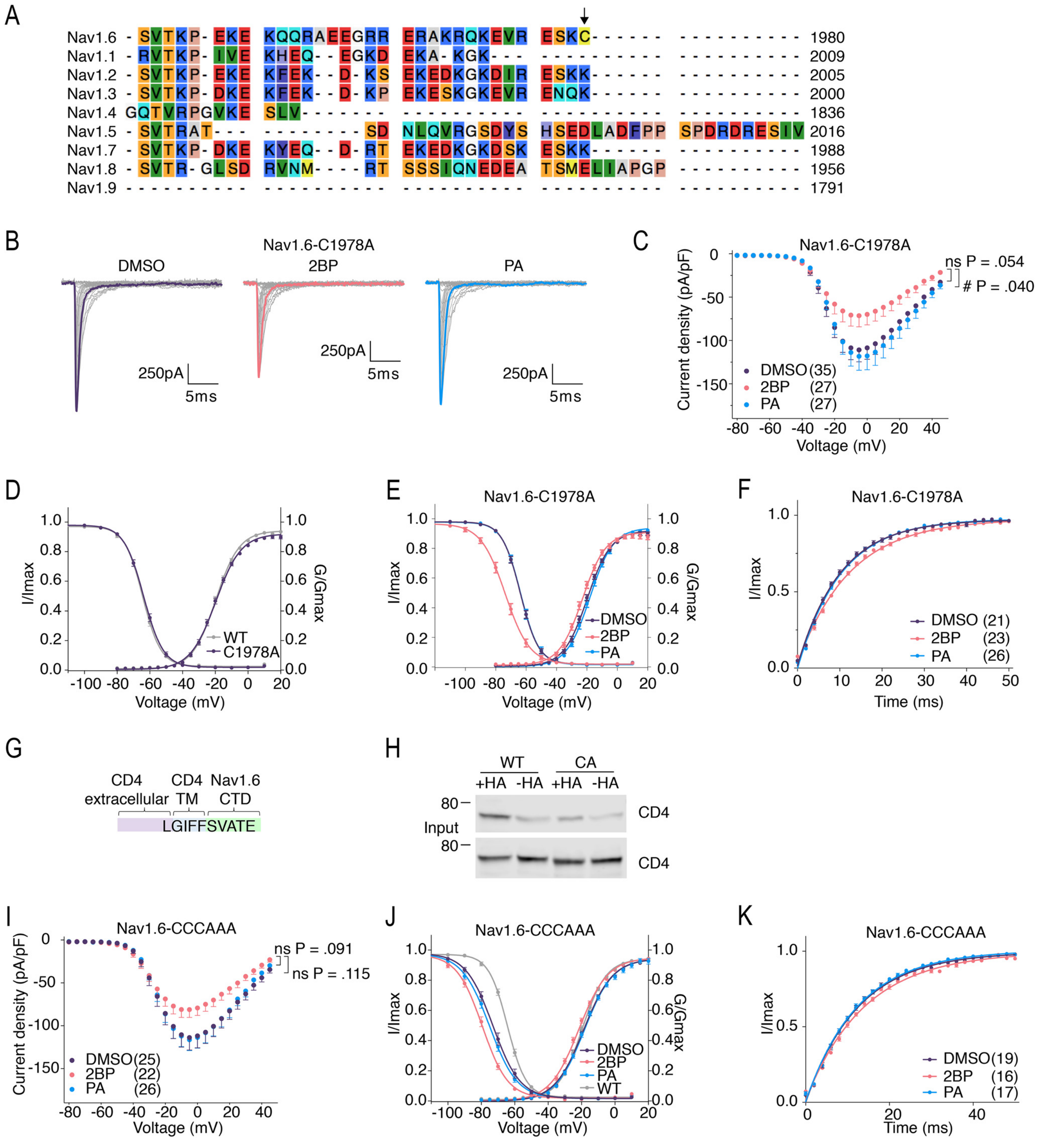

Figure 4. C1978A eliminates Nav1.6 current enhancement by PA without altering voltage dependence response to *S*-palmitoylation manipulation. *A*, a segment of amino acid alignment of the Nav family. The *arrow* indicates Cys[1978] in Nav1.6. *B*, representative current traces elicited from Nav1.6–C1978A with different treatments. *C* and *I*, current density–voltage plots of Nav1.6–C1978A and Nav1.6–CCCAAA. #, $p < 0.05$ PA compared with 2BP in two-way ANOVA. *D*, *E*, and *J*, steady-state inactivation and activation curves of Nav1.6–C1978A and Nav1.6–CCCAAA fitted with Boltzmann functions. *F* and *K*, recovery from inactivation of Nav1.6–C1978A and Nav1.6–CCCAAA with recovery time duration from 0 to 50 ms. The data are presented as means ± S.E. The values and statistical significance are reported in Table 1. *G*, schematic illustration of the CD4–Nav1.6–CTD fusion protein showing the last five amino acids of the CD4 transmembrane segment and the first five amino acids of the Nav1.6–CTD. *H*, acyl-biotin exchange assays on WT and C1978A fusion protein-transfected HEK cells probed with CD4 antibody.

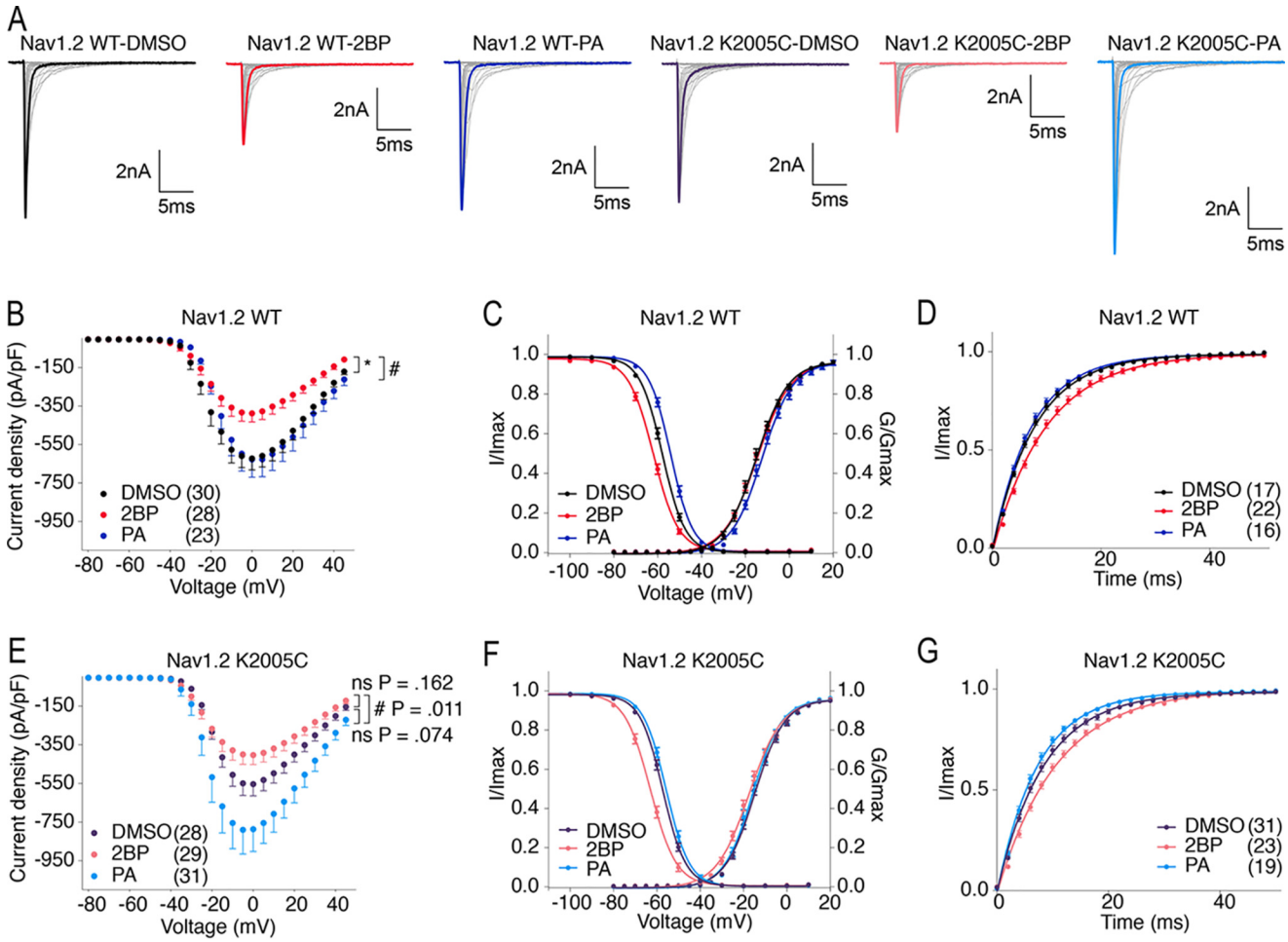

Figure 5. An exogenous cysteine renders Nav1.2 current amplitude enhanced by *S*-palmitoylation. Voltage-clamp recordings from ND7/23 cells transiently transfected with Nav1.2r–WT and Nav1.2r–K2005C are shown. Transfected cells were treated with DMSO as solvent control, 2BP to block *S*-palmitoylation, and PA to enhance *S*-palmitoylation 24 h before recording. *A*, representative current traces from different treatment groups elicited by activation protocol. *B* and *E*, current density–voltage plots. *, $p < 0.05$ compared with DMSO, #, $p < 0.05$ PA compared with 2BP in two-way ANOVA. *C* and *F*, steady-state inactivation and activation curves fitted with a Boltzmann function. *D* and *G*, recovery from inactivation with recovery time duration from 0 to 50 ms. The data are presented as means ± S.E. The values and statistical significance are reported in Table 1.

($V_{½}$ = −54.01 ± 0.10 mV; p = 0.0003) (Fig. 5*C*), similar to previous results obtained from *Xenopus* oocytes expressing Nav1.2 (10). With these data, we demonstrate that Nav1.2 fails to display sensitivity to current enhanced by *S*-palmitoylation but preserves the voltage dependence modulation conveyed by the conserved double cysteines in loop 2.

To further explore the role of *S*-palmitoylation at the C terminus of a voltage-gated sodium channel other than Nav1.6, we introduced an exogenous cysteine to Nav1.2 at its C-terminal end point (Lys^{2005}). Fig. 5*A* shows the representative traces of TTXr Nav1.2–K2005C currents. We observed that Nav1.2–K2005C displays the bidirectional current density modulation produced by 2BP and PA treatments (Fig. 5*E*) similar to Nav1.6–WT (Fig. 2*C*), suggesting that *S*-palmitoylation at the C-terminal exogenous cysteine in Nav1.2 alters the Nav1.2 current density response to *S*-palmitoylation modulation treatments. This indicates that the functional importance of *S*-palmitoylation at this position has the potential to apply to multiple Nav isoforms. However, the bidirectional modulation of Nav1.2 current is not as dramatic as that observed in Nav1.6. This might be due to a lower *S*-palmitoylation efficiency in Nav1.2, possibly because of the difference in sequence environment, protein conformation, and/or interacting partners associated with the channel. Unexpectedly, the pattern of voltage dependence response of Nav1.2–K2005C is more similar to Nav1.6–WT rather than Nav1.2–WT (Fig. 5*F*): increasing *S*-palmitoylation substrate availability with PA treatment does not depolarize the voltage dependence of steady-state inactivation in Nav1.2–K2005C (PA: $V_{½}$ = −55.57 ± 0.22 mV *versus* DMSO: $V_{½}$ = −57.20 ± 0.19 mV; p = 0.2877), whereas blocking *S*-palmitoylation with 2BP causes a hyperpolarizing shift in the voltage dependence of steady-state inactivation ($V_{½}$ = −62.91 ± 0.26 mV; $p < 0.0001$). The loss of voltage dependence modulation in response to PA supplementation could be caused by the introduction of an extra *S*-palmitoylation site. This is in contrast to Nav1.6, where the *S*-palmitoylation status of the two sites seem to be independent, further supporting our hypothesis that *S*-palmitoylation modifies Nav functions in an isoform-dependent manner. Moreover, our data also suggest that whether 2BP and PA individual treatments can lead to appreciable effects also depends on the saturation level of *S*-palmitoylation at specific sites: if saturated, possibly as in the case of Cys^{1169} and Cys^{1170} in Nav1.6, increasing

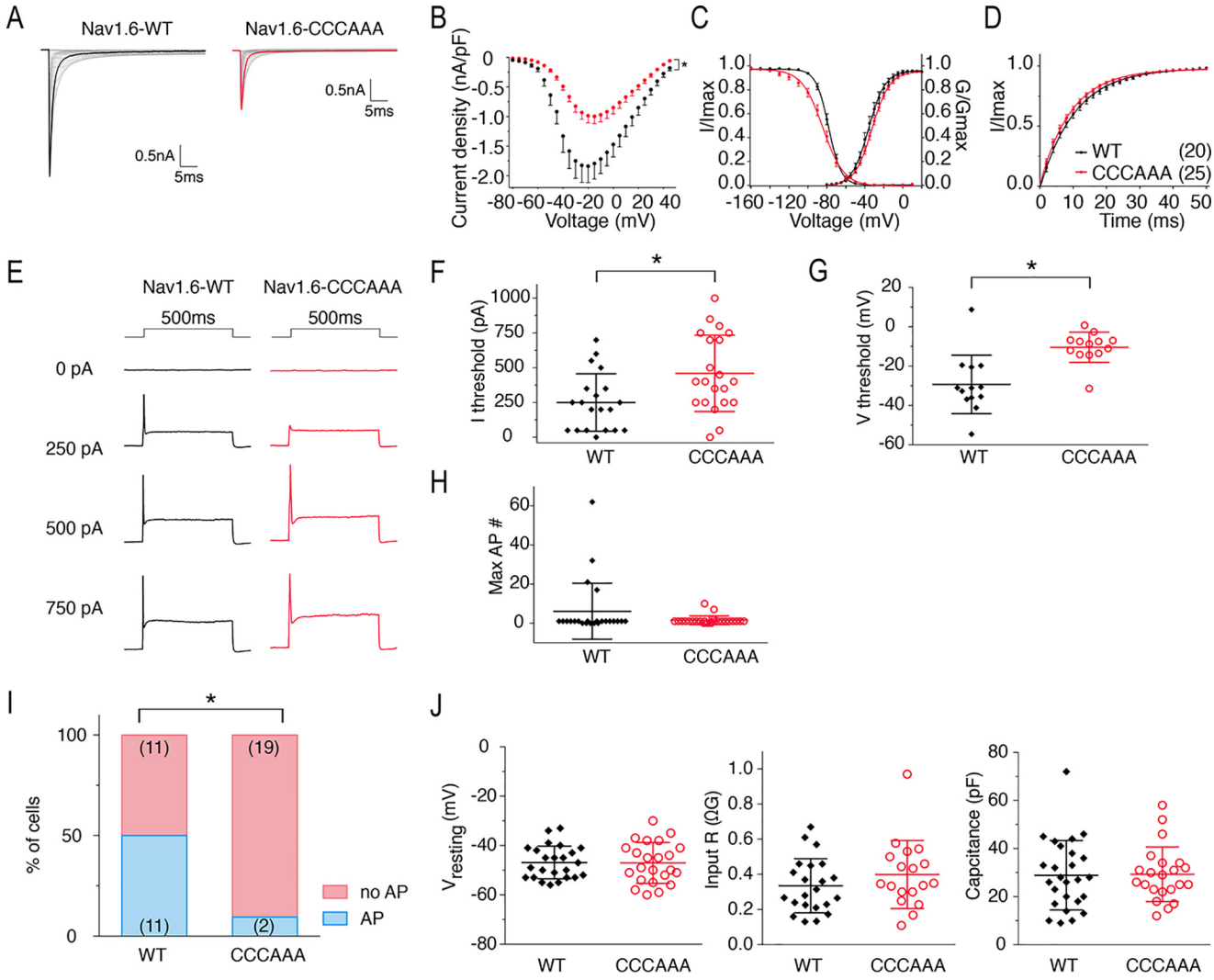

Figure 6. Loss of *S*-palmitoylation at Cys^{1169}, Cys^{1170}, and Cys^{1978} reduced Nav1.6 current and channel availability and dampened Nav1.6-mediated excitability in DRG neuron. *A*, representative TTXr current traces elicited from Nav1.6–WT and Nav1.6–CCCAAA transfected DRG neurons with endogenous Nav1.8 knocked down. *B*, current density–voltage plot. *, $p < 0.05$ in two-way ANOVA. *C*, steady-state inactivation and activation curves fitted with Boltzmann functions. *D*, recovery from inactivation with recovery time duration from 0 to 50 ms. The data are presented as means ± S.E. in *B–D*. The values and statistical significance are reported in Table 1. *E*, representative traces of stimulated action potentials from Nav1.6–WT and Nav1.6–CCCAAA transfected DRG neurons with endogenous Nav1.8 knocked down. *F* and *G*, current and voltage thresholds for evoked action potential during 500-ms stimulation. *, $p < 0.05$ in *t* test. *H*, maximum number of evoked action potentials during 500-ms stimulations from 0 to 1000 pA in 50-pA increments. *I*, percentage of cells fired *versus* did not fire action potential upon 1-ms stimulations from 0 to 1000 pA in 50-pA increments. *, $p < 0.05$ in χ^2 test. *J*, resting membrane potential, input resistance and cell capacitance of Nav1.6–WT and Nav1.6–CCCAAA transfected DRG neurons. The data are presented as means ± S.D. in *F–H* and *J*.

S-palmitoylation substrate availability would not show an appreciable effect on channel properties, whereas if a *S*-palmitoylation site is nonsaturated, likely the case with the double cysteines in Nav1.2–loop 2 and Cys^{1978} in Nav1.6, manipulating the *S*-palmitoylation status of the channels with 2BP and PA treatments results in bidirectional effects.

Loss of S-palmitoylation at Cys^{1169}, Cys^{1170}, and Cys^{1978} in Nav1.6 reduces channel activity and dampens Nav1.6-mediated excitability in DRG neuron

To investigate how loss of *S*-palmitoylation at Cys^{1169}, Cys^{1170}, and Cys^{1978} impacts Nav1.6 activity in neurons, we compared the properties of transfected Nav1.6r–WT and Nav1.6r–CCCAAA channels in DRG neurons. The use of adult DRG neurons was specifically advantageous for our study because of the ease of transient transfection and high expression level of recombinant Nav1.6 we could achieve with this method. Because Nav1.8 is the major TTXr sodium channel in DRG neurons, Nav1.6r–WT and Nav1.6r–CCCAAA cDNA constructs were co-transfected with Nav1.8-targeting shRNA to knock down the endogenous Nav1.8 channels (27). DRG neurons express multiple TTX-sensitive sodium channels (including Nav1.6 (28)), and therefore transfected Nav1.6r current was isolated by applying 500 nM TTX in the extracellular solution in patch clamp recordings. We found that DRG neurons expressing Nav1.6–CCCAAA conduct smaller TTXr sodium currents (Fig. 6, *A* and *B*), and these currents have a hyperpolarizing shift of steady-state inactivation compared with the Nav1.6–WT transfected neurons (Fig. 6*C*).

Next we examined the Nav1.6-mediated excitability in DRG neurons. We observed a higher current threshold (Fig. 6*F*, CCCAAA: 459.5 ± 59.82 pA *versus* WT: 250.0 ± 46.17 pA;

$p = 0.0089$), as well as a higher voltage threshold (Fig. 6*G*, CCCAAA: −10.42 ± 2.136 mV *versus* WT: −29.27 ± 4.123 mV; $p = 0.0007$) for evoked action potential in the Nav1.6–CCCAAA transfected neurons with 500-ms stimulations compared with Nav1.6–WT transfected neurons. The maximum number of action potentials fired during the 500-ms stimulation are not different (Fig. 6*H*). This is because in our experiments most of the DRG neurons fire only one action potential with endogenous Nav1.8 knocked down. However, we found that fewer Nav1.6–CCCAAA transfected neurons are able to fire an action potential upon a 1-ms stimulation up to 1 nA compared with WT transfected neurons (Fig. 6*I*, AP/total cell count, WT: 11 of 22 *versus* CCCAAA: 2 of 21, $p = 0.0039$ in χ^2 test). Collectively, these data suggest that loss of *S*-palmitoylation at Cys^{1169}, Cys^{1170}, and Cys^{1978} reduces Nav1.6 activity and dampens Nav1.6-mediated excitability in DRG neurons. Importantly, this was not due to any difference in intrinsic properties (resting membrane potential, input resistance, and cell capacitance) between WT- and CCCAAA-transfected neurons (Fig. 6*J*).

Discussion

We show here that Nav1.6 is modified by *S*-palmitoylation. Three major *S*-palmitoylation sites are identified: the two adjacent cysteines in loop 2, Cys^{1169} and Cys^{1170}, and the C-terminal Cys^{1978}. The two cysteines in loop 2 are highly conserved among Nav isoforms (Fig. 3*A*), but their functional significance can vary: in Nav1.6 (Fig. 3) and Nav1.2 (Fig. 5 and Ref. 10), *S*-palmitoylation at the conserved cysteines modulates channel steady-state inactivation; in Nav1.5, similar modulation is mediated by *S*-palmitoylation at a nonconserved residue (Cys^{981}) without involving the conserved cysteines (9). This suggests that the function of a *S*-palmitoylation site in a voltage-gated sodium channel depends on the specific isoform. It is also possible that *S*-palmitoylation may not ubiquitously occur at conserved sites in all Nav isoforms.

We also demonstrate that *S*-palmitoylation regulates distinct Nav1.6 functions by modifying different cysteine residues in the channel. Without affecting steady-state inactivation, the *S*-palmitoylation status of Cys^{1978} substantially modulates the current amplitude of Nav1.6 (Fig. 4). This uncovers the possibility to fine-tune specific channel properties by modulating *S*-palmitoylation at respective residues. The underlying mechanism of current amplitude regulation might be that *S*-palmitoylation at Nav1.6–Cys^{1978} promotes the surface expression of the channel. However, we were not able to directly test this hypothesis because of the extremely low expression level of Nav1.6 in our heterologous system.

Intriguingly, the C-terminal cysteine is unique to Nav1.6 and absent from all other Nav isoforms (Fig. 4*A*). More importantly, this residue is invariant in Nav1.6 among most mammalian and vertebrate species with only a few exceptions in lower vertebrates (Fig. S1*B*). From an evolutionary perspective, this conservation indicates that Cys^{1978} is a more recent adaptation for Navs and probably confers critical regulation that is specific to Nav1.6 and to its special physiological role. Indeed, we observed current enhancement by *S*-palmitoylation only in the presence of the C-terminal cysteine in Nav1.6. Nav1.2, lacking the homologous *S*-palmitoylation site, only obtained such modulation when an exogenous cysteine was introduced (K2005C) (Fig. 5). It is noteworthy that the beginning two-thirds of the CTD is quite conserved among all human Nav isoforms, whereas the remaining third that follows the calmodulin-binding IQ motif is highly variable. Thus, it is reasonable to speculate that the last third of the CTD, which includes the unique *S*-palmitoylation site in Nav1.6, serves isoform-dependent functions for Nav channels.

It is important to point out that the effect size of current enhancement in Nav1.2–K2005C is far smaller than that in Nav1.6, possibly because of lower *S*-palmitoylation efficiency at an exogenous *S*-palmitoylation site or due to other C-terminal isoform-specific differences. There is growing evidence that there is enzyme–substrate specificity for *S*-palmitoylation (29–34). PATs, the enzymes that catalyze the *S*-palmitoylation reaction, may recognize their substrates based on protein secondary structure (35) and/or protein–protein interacting domains (30, 31, 36–38), although these PATs were once deemed stochastic because a consensus sequence motif has yet to emerge (39). The existence of PAT–substrate specificity is further supported by our observation of suboptimal effect of current enhancement by *S*-palmitoylation on an exogenous site in Nav1.2–K2005C (Fig. 5) along with the possible lack of *S*-palmitoylation at the conserved double cysteines in Nav1.5 (9).

So far, 23 human PATs have been identified. It has been shown that these PATs differ in tissue, cell type, and subcellular distribution (16, 37, 40–43), creating a spatial, and thus functional segregation among these enzymes. Additionally, PAT distributions are subject to dynamic regulation (7), adding another layer of complexity for the regulation of *S*-palmitoylation. Although more work is needed to clarify the mechanisms of *S*-palmitoylation and its regulation, the intricacy of PAT specificity and the variety of *S*-palmitoylation functionalities substantiate its potential of being exploited to target Navs with isoform specificity.

Our discovery of Nav1.6 modification by *S*-palmitoylation provides a novel strategy to modulate neuronal excitability, considering the crucial role of Nav1.6 in action potential initiation and propagation in both CNS and peripheral nervous system. We demonstrated, as a proof of concept, that altering *S*-palmitoylation of Nav1.6 exerts significant impact on the excitability of adult DRG neurons (Fig. 6). The DRG neurons provide important advantages for the purpose of our study. Adult DRG neurons can express high levels of recombinant Nav1.6 via transient transfection (44), and adult neurons can be used for both voltage-clamp characterization of isolated ionic currents and current clamp analysis of excitability (45). On the contrary, in our experience, the vast majority of cultured CNS neurons are either too immature to support a sufficient level of Nav1.6 expression (because Nav1.6 is an adult brain isoform that starts its expression relatively late in development) or too difficult to transfect. Moreover, the need for transient transfection of Nav1.6 and its *S*-palmitoylation– deficient variants is imposed by the fact that pharmacological treatments (2BP and PA) affect global *S*-palmitoylation of a wide range of neuronal proteins, and thus it is impossible to isolate the effect of altering

Nav1.6 *S*-palmitoylation using a pharmacological approach to manipulate palmitoylation in neurons. DRG neurons are not a perfect neuronal environment to demonstrate the functional significance of Nav1.6 *S*-palmitoylation on excitability. Although endogenous Nav1.6 expression is detected in DRG neurons (28), Nav1.6 has a more prominent role in setting the excitatory tone of central neurons. Thus, it may be highly desirable to further evaluate the impact of Nav1.6 *S*-palmitoylation on central neuron activity in future studies, possibly using transgenic mice with a specific palmitoylation site knocked out. Additionally, the requirement for knocking down the endogenous TTXr Nav1.8 to isolate the effect of Nav1.6 rendered the majority of DRG neurons unable to fire multiple action potentials under our experimental conditions. The DRG neurons endogenously express a combination of TTX-sensitive (Nav1.6 and Nav1.7) and TTXr (mainly Nav1.8) sodium currents (46). It is well-established that Nav1.6 and Nav1.7 mainly conduct subthreshold sodium currents and set the threshold for action potentials, whereas Nav1.8 is the major contributor to action potential upstroke and repetitive firing in the DRG neurons (46). Although Nav1.6 supports high frequency, repetitive firing in a wide range of CNS neurons (47–53), the cellular background of DRG neurons, including the subset of K^+ channels, the leaky soma membrane property, the post-translational modifications, and possibly distinct combination of Nav1.6 interacting proteins presented, may limit the ability of this channel to generate multiple action potentials on its own. Finally, although the use of DRG neurons for Nav1.6 expression provided a clear picture of the role of *S*-palmitoylation in modulating Nav1.6-mediated excitability, it does not reflect the firing behavior of DRG neuron *in vivo*.

Nav1.6 has long been an attractive target for excitability modulation because of its unique properties that support high frequency, repetitive firing in a wide range of neurons (47–52, 54). Moreover, Nav1.6 is distinguished by its ability to generate high levels of persistent current (47, 55) and resurgent current (56, 57), which are often perturbed (usually augmented) in channelopathies. Over 200 disease mutations are reported in ClinVar (58) for Nav1.6, implicating its direct involvement in the etiology of diverse neurological diseases including epilepsy, cognitive deficit, and movement disorders. Although none of them directly removes or introduces a Nav1.6 *S*-palmitoylation site, disease mutations that are seemingly distant from a *S*-palmitoylation site may influence *S*-palmitoylation by altering the post-translational code (59), changing the secondary structure, or disrupting protein–protein interaction. Additionally, there can be complex interplays between different post-translational interactions (5, 60–64). Thus, mutations that interfere with, for example, phosphorylation or its related signaling pathways might also affect *S*-palmitoylation and indirectly alter channel maturation, trafficking, and functional properties. Conversely, altering *S*-palmitoylation status of specific sites offers an opportunity to attenuate abnormal Nav1.6 activity imposed by disease mutations. Collectively, we present *S*-palmitoylation as a novel mechanism for isoform-specific regulation for voltage-gated sodium channels and propose a new therapeutic strategy to modulate excitability disorders.

Experimental procedures

DNA constructs

pcDNA3–Nav1.6r was modified from a pcDNA3–Nav1.6r–EGFP construct (23) with a stop codon inserted before the EGFP sequence. This Nav1.6 channel has been rendered resistant to TTX (Nav1.6r) by a Y371S substitution. pcDNA3–Nav1.2 construct was rendered resistant to TTX by a F385S substitution. Fusion proteins CD4–Nav1.6–loop 2 and CD4–Nav1.6–CTD were designed in-house and purchased from GenScript. Briefly, the extracellular and transmembrane segments of CD4 (amino acid 1–418) were fused with Nav1.6–loop 2 (amino acid 976–1193) or Nav1.6–CTD (amino acid 1768–1978). All mutations (Nav1.6 C1169A/C1170A, Nav1.6 C1978A, Nav1.2 K2005C, CD4–CTD CA, and CD4–loop 2 CCAA) were introduced into the WT cDNA constructs using a QuikChange II XL site-directed mutagenesis kit from Agilent Technologies according to the manufacturer's instructions. Mutant constructs were fully sequenced (ACGT, Inc.) to confirm correct mutation and absence of additional mutations.

Cell culture and transfection

The neuronal cell line ND7/23 was used to transiently express WT and mutant Nav1.6r and Nav1.2r channels for functional characterization; the HEK 293 cell line was used to transiently express WT and mutant CD4–Nav1.6 fusion proteins and to stably express Nav1.6 for acyl-biotin exchange assays. The cells were grown under standard tissue culture conditions and were transfected using Invitrogen Lipofectamine 2000 transfection reagent according to the manufacturer's instructions. Briefly, the lipid–DNA mixture (5-μg channel construct and 0.5-μg enhanced GFP (EGFP) construct) in Opti-MEM medium was added to cells for 4 h, after which transfected cells were split onto a 35-mm dish with fresh medium. Transfected cells were incubated at 30 °C overnight to increase channel surface expression. 24–32 h after transfection, whole-cell voltage-clamp recordings were performed. Transfected cells were identified by EGFP expression under a fluorescent microscope. To manipulate *S*-palmitoylation status, 25 μM 2BP, 10 μM PA, or DMSO were added to medium 8 h after transfection for overnight incubation.

Rat DRG neurons were dissociated and cultured as previously described (65). Briefly, young adult male Sprague-Dawley rats, in adherence with animal procedures approved by the Indiana University School of Medicine and the School of Science Institutional Animal Care and Use Committees, were euthanized by carbon dioxide overexposure followed by decapitation. All DRGs were harvested and subsequently incubated in collagenase (1 mg/ml) and protease (1 mg/ml) for 70 min. DRGs were then spun down and washed in Dulbecco's modified Eagle's medium with 10% fetal bovine serum. After trituration, the cells were plated on coverslips coated with poly-D-lysine and laminin. Transient transfection was performed using the Helios Gene Gun (Bio-Rad) as previously described (57, 66). The cells were co-transfected with Nav1.6r cDNA and Nav1.8 shRNA with an internal ribosome entry site–EGFP. Previous

data have shown that the Nav1.8 shRNA reduces endogenous Nav1.8 current in DRG neurons by 98% (27, 57). Patch clamp recordings were performed 48 h after transfection.

Acyl-biotin exchange

Performed as previously described with minor modifications (9, 67). Briefly, HEK 293 cells stably expressing Nav1.6 or transiently transfected with WT CD4–loop 2, CD4–CTD and their mutant variants were lysed and treated with *N*-ethylmaleimide overnight to block free cysteines at 4 °C with end-to-end rotation. The next day, *N*-ethylmaleimide was removed by chloroform-methanol precipitation and dissolved in 4% SDS buffer. The soluble protein was then divided into two equal parts and treated with either NH_2OH (0.7 M hydroxylamine, 1 mM biotin, 0.2% Triton X-100, and 1× protease inhibitor) or Tris-buffered solution (200 mM Tris, 1 mM biotin, 0.2% Triton X-100, and 1× protease inhibitor). The reaction was carried out in the dark for 1 h. Chemicals were removed by chloroform-methanol precipitation. Protein was resolubilized in 2% SDS buffer and subsequently diluted with lysis buffer to achieve 0.1% SDS concentration for streptavidin-agarose bead capture. BCA protein assay was performed to ensure that equal amount of proteins from different groups were subjected to the streptavidin-agarose beads capture. After 1 h of incubation at room temperature, the beads were washed four times with lysis buffer containing 1% Triton X-100 and 0.1% SDS. Protein was eluted in LDS sample buffer (Invitrogen) with 2% β-mercaptoethanol and heated at 65 °C for 5 min before probing with Western blotting.

Gel electrophoresis and Western immunoblotting

Gel electrophoresis and protein transfer was performed according to the standard protocol (Life Technologies). Primary antibodies include mouse pan-Nav antibody (Sigma, 1:1000) and rabbit CD4 antibody (Abcam, 1:2000). Fluorescently labeled secondary antibodies used were goat anti-mouse IgG H&L IRDye® 800CW (Abcam, 1:20000) and goat anti-rabbit IgG IRDye 800CW (Li-Cor, 1:10000).

Whole-cell patch clamp recordings

All recordings were obtained at room temperature (~22 °C) using a HEKA EPC-10 amplifier and the PatchMaster program (v2 × 73.2, HEKA Electronic) as previously described (68). For voltage-clamp recordings, electrodes were fabricated from 1.7-mm capillary glass and fire-polished to a resistance of 0.8–1.0 MΩ using a Sutter P-1000 micropipette puller (Sutter Instrument Company). The series of recording protocols was started 3 min after break-in for each cell, which controlled for time-dependent shifts in channel properties. The cells were not considered for analysis if the initial seal resistance was <1 GΩ or if they had a series resistance of >3 MΩ. Voltage errors were minimized using >80% series resistance compensation, and passive leak currents were cancelled by subtraction. The intracellular solution contained 140 mM CsF, 10 mM NaCl, 1.1 mM EGTA, and 10 mM HEPES, adjusted to a pH of 7.30 with CsOH. For recordings in ND7/23 cells, the extracellular solution contained 140 mM NaCl, 20 mM TEA-Cl, 3 mM KCl, 1 mM $MgCl_2$, 1 mM $CaCl_2$, and 10 mM HEPES, adjusted to a pH of 7.30 with NaOH. For recordings in DRG neurons, the extracellular solution contained 140 mM NaCl, 20 mM TEA-Cl, 3 mM KCl, 1 mM $MgCl_2$, 1 mM $CaCl_2$, 0.1 mM $CdCl_2$, and 10 mM HEPES, adjusted to a pH of 7.30 with NaOH. 500 nM TTX was added to the extracellular solution to block endogenous sodium currents and isolate TTX-resistant current generated by transfected channels. Osmolarity of all solutions was adjusted to 300 mOsm.

For current-clamp recordings, electrodes were fabricated from 1.2-mm capillary glass to achieve a resistance of 4.0–6.0 MΩ. The series of recording protocols was started 2 min after break-in for each cell. The intracellular solution contained 140 mM KCl, 5 mM $MgCl_2$, 5 mM EGTA, 2.5 mM $CaCl_2$, and 10 mM HEPES, adjusted to a pH of 7.30 with KOH. The extracellular solution contained 140 mM NaCl, 5 mM KCl, 2 mM $CaCl_2$, 1 mM MgCl, and 10 mM HEPES, adjusted to a pH of 7.30 with NaOH. Osmolarity of solutions was adjusted to 300 mOsm.

Patch-clamp protocols and data analysis: activation protocol

Transient sodium current (I_{NaT}) was measured during a 50-ms depolarizing step (−80 to +45 mV; 5-mV increment) from a holding potential of −120 mV. The current density was calculated by dividing the measured I_{NaT} by the capacitance of the cell. Sodium current conductance (G_{Na}) was converted from I_{NaT} using the equation $G_{Na} = I_{NaT}/(V - V_{rev})$, where V_{rev} is the reversal potential of Na^+ obtained in FitMaster (v2 × 73.5, HEKA Electronic) for each cell. Activation curves were generated by plotting normalized G_{Na} against depolarizing potentials and fitting it with the Boltzmann function in the form of $G_{Na}/G_{max} = 1/(1 + \exp[(V_{50,act} - V)/k_{act}])$, where G_{max} is the maximal G_{Na}, $V_{50,act}$ is the potential at which activation is half-maximal, V is the depolarizing potential, and k_{act} is the slope factor.

Steady-state inactivation

Availability of sodium channels was measured by the peak sodium current during a 20-ms test pulse at 0 mV following a 500-ms prepulse (−140 to +10 mV; 10-mV increment) that allows channels to enter equilibrium states. Steady-state inactivation curves were generated by plotting normalized sodium current against prepulse potentials and fitting it with the Boltzmann function in the form of $I/I_{max} = 1/(1 + \exp[(V_{50,inact} - V)/k_{inact}])$, where I_{max} is the maximal sodium current obtained in this protocol, $V_{50,inact}$ is the potential at which half of the sodium channels are available for activation, V is the prepulse potential, and k_{inact} is the slope factor.

Recovery from inactivation

A 20-ms depolarization prepulse at 0 mV was applied to allow channel activation and subsequent inactivation, which was followed by a repolarizing step to −80 mV for durations ranging from 0 to 50 ms with 2-ms increment. The noninactivated sodium currents were measured during a subsequent 20-ms test pulse at 0 mV and normalized to the maximum current obtained in this protocol. The normalized noninactivated sodium current was plotted against the duration of

repolarizing step and fitted with a single exponential function.

Statistics

GraphPad Prism (v 6.00, GraphPad Software) was used for statistical analysis and curve fitting with the nonlinear least-squares minimization method. The data acquired from voltage-clamp recording are presented as means ± S.E. of the indicated number of cells (*n*). The data acquired from current-clamp recording are presented as means ± S.D. and plotted with individual values. For comparisons of current density from both ND7/23 cells and DRG neurons, two-way ANOVA was performed. For comparisons of all the other parameters, one-way ANOVA followed by Tukey multiple comparisons test was performed for treatment groups in the same channel variant transfected in ND7/23 cells; Student's *t* test was performed for WT and individual mutant channels transfected in ND7/23 cells and DRG neurons.

Author contributions—Y. P., Y. X., Z. P., and T. R. C. conceptualization; Y. P. data curation; Y. P. formal analysis; Y. P. investigation; Y. P., Y. X., and Z. P. methodology; Y. P. writing-original draft; Y. X. and T. R. C. supervision; T. R. C. funding acquisition; T. R. C. writing-review and editing.

References

1. Catterall, W. A. (2012) Voltage-gated sodium channels at 60: structure, function and pathophysiology. *J. Physiol.* **590,** 2577–2589 CrossRef Medline
2. Shen, H., Liu, D., Wu, K., Lei, J., and Yan, N. (2019) Structures of human Nav1.7 channel in complex with auxiliary subunits and animal toxins. *Science* **363,** 1303–1308 CrossRef Medline
3. Pan, X., Li, Z., Huang, X., Huang, G., Gao, S., Shen, H., Liu, L., Lei, J., and Yan, N. (2019) Molecular basis for pore blockade of human Na^+ channel Nav1.2 by the μ-conotoxin KIIIA. *Science* **363,** 1309–1313 CrossRef Medline
4. Bagal, S. K., Marron, B. E., Owen, R. M., Storer, R. I., and Swain, N. A. (2015) Voltage gated sodium channels as drug discovery targets. *Channels* **9,** 360–366 CrossRef Medline
5. Pei, Z., Pan, Y., and Cummins, T. R. (2018) Posttranslational modification of sodium channels. *Handb. Exp. Pharmacol.* **246,** 101–124 Medline
6. Naumenko, V. S., and Ponimaskin, E. (2018) Palmitoylation as a functional regulator of neurotransmitter receptors. *Neural Plasticity* **2018**
7. Globa, A. K., and Bamji, S. X. (2017) Protein palmitoylation in the development and plasticity of neuronal connections. *Curr. Opin. Neurobiol.* **45,** 210–220 CrossRef Medline
8. Fukata, Y., and Fukata, M. (2010) Protein palmitoylation in neuronal development and synaptic plasticity. *Nat. Rev. Neurosci.* **11,** 161–175 CrossRef Medline
9. Pei, Z., Xiao, Y., Meng, J., Hudmon, A., and Cummins, T. R. (2016) Cardiac sodium channel palmitoylation regulates channel availability and myocyte excitability with implications for arrhythmia generation. *Nat. Commun.* **7,** 12035 CrossRef Medline
10. Bosmans, F., Milescu, M., and Swartz, K. J. (2011) Palmitoylation influences the function and pharmacology of sodium channels. *Proc. Natl. Acad. Sci. U.S.A.* **108,** 20213–20218 CrossRef Medline
11. Itoh, M., Okuno, H., Yamada, D., Yamashita, M., Abe, M., Natsume, R., Kaizuka, T., Sakimura, K., Hoshino, M., Mishina, M., Wada, K., Sekiguchi, M., and Hayashi, T. (2019) Perturbed expression pattern of the immediate early gene Arc in the dentate gyrus of GluA1 C-terminal palmitoylation-deficient mice. *Neuropsychopharmacol. Rep.* **39,** 61–66 Medline
12. Itoh, M., Yamashita, M., Kaneko, M., Okuno, H., Abe, M., Yamazaki, M., Natsume, R., Yamada, D., Kaizuka, T., Suwa, R., Sakimura, K., Sekiguchi, M., Wada, K., Hoshino, M., Mishina, M., *et al.* (2018) Deficiency of AMPAR–palmitoylation aggravates seizure susceptibility. *J. Neurosci.* **38,** 10220–10235 CrossRef Medline
13. Hayashi, T., Rumbaugh, G., and Huganir, R. L. (2005) Differential regulation of AMPA receptor subunit trafficking by palmitoylation of two distinct sites. *Neuron* **47,** 709–723 CrossRef Medline
14. Chien, A. J., Carr, K. M., Shirokov, R. E., Rios, E., and Hosey, M. M. (1996) Identification of palmitoylation sites within the L-type calcium channel β2a subunit and effects on channel function. *J. Biol. Chem.* **271,** 26465–26468 CrossRef Medline
15. Roth, A. F., Wan, J., Bailey, A. O., Sun, B., Kuchar, J. A., Green, W. N., Phinney, B. S., Yates, J. R., 3rd, Davis, N. G. (2006) Global analysis of protein palmitoylation in yeast. *Cell* **125,** 1003–1013 CrossRef Medline
16. Fukata, M., Fukata, Y., Adesnik, H., Nicoll, R. A., and Bredt, D. S. (2004) Identification of PSD-95 palmitoylating enzymes. *Neuron* **44,** 987–996 CrossRef Medline
17. Ponimaskin, E., Dityateva, G., Ruonala, M. O., Fukata, M., Fukata, Y., Kobe, F., Wouters, F. S., Delling, M., Bredt, D. S., Schachner, M., and Dityatev, A. (2008) Fibroblast growth factor-regulated palmitoylation of the neural cell adhesion molecule determines neuronal morphogenesis. *J. Neurosci.* **28,** 8897–8907 CrossRef Medline
18. Lievens, P. M.-J., Kuznetsova, T., Kochlamazashvili, G., Cesca, F., Gorinski, N., Galil, D. A., Cherkas, V., Ronkina, N., Lafera, J., Gaestel, M., Ponimaskin, E., and Dityatev, A. (2016) ZDHHC3 tyrosine phosphorylation regulates neural cell adhesion molecule palmitoylation. *Mol. Cell. Biol.* **36,** 2208–2225 CrossRef Medline
19. Brigidi, G. S., Sun, Y., Beccano-Kelly, D., Pitman, K., Mobasser, M., Borgland, S. L., Milnerwood, A. J., and Bamji, S. X. (2014) Palmitoylation of δ-catenin by DHHC5 mediates activity-induced synapse plasticity. *Nat. Neurosci.* **17,** 522–532 CrossRef Medline
20. Noritake, J., Fukata, Y., Iwanaga, T., Hosomi, N., Tsutsumi, R., Matsuda, N., Tani, H., Iwanari, H., Mochizuki, Y., Kodama, T., and Matsuura, Y., Bredt, D. S., Hamakubo, T., and Fukata, M. (2009) Mobile DHHC palmitoylating enzyme mediates activity-sensitive synaptic targeting of PSD-95. *J. Cell Biol.* **186,** 147–160 CrossRef Medline
21. Wood, J. N., Bevan, S. J., Coote, P. R., Dunn, P. M., Harmar, A., Hogan, P., Latchman, D. S., Morrison, C., Rougon, G., and Theveniau, M. (1990) Novel cell lines display properties of nociceptive sensory neurons. *Proc. Biol. Sci.* **241,** 187–194 CrossRef Medline
22. Rogers, M., Zidar, N., Kikelj, D., and Kirby, R. W. (2016) Characterization of endogenous sodium channels in the ND7–23 neuroblastoma cell line: implications for use as a heterologous ion channel expression system suitable for automated patch clamp screening. *Assay Drug Dev. Technol.* **14,** 109–130 CrossRef Medline
23. Gasser, A., Ho, T. S., Cheng, X., Chang, K.-J., Waxman, S. G., Rasband, M. N., and Dib-Hajj, S. D. (2012) An ankyrin G–binding motif is necessary and sufficient for targeting Nav1.6 sodium channels to axon initial segments and nodes of Ranvier. *J. Neurosci.* **32,** 7232–7243 CrossRef Medline
24. Ren, J., Wen, L., Gao, X., Jin, C., Xue, Y., and Yao, X. (2008) CSS-Palm 2.0: an updated software for palmitoylation sites prediction. *Protein Eng. Des. Sel.* **21,** 639–644 CrossRef Medline
25. Jindal, H. K., Folco, E. J., Liu, G. X., and Koren, G. (2008) Posttranslational modification of voltage-dependent potassium channel Kv1.5: COOH-terminal palmitoylation modulates its biological properties. *Am. J. Physiol. Heart Circ. Physiol.* **294,** H2012–H2021 CrossRef Medline
26. Hayashi, T., Thomas, G. M., and Huganir, R. L. (2009) Dual palmitoylation of NR2 subunits regulates NMDA receptor trafficking. *Neuron* **64,** 213–226 CrossRef Medline
27. Barbosa, C., Tan, Z.-Y., Wang, R., Xie, W., Strong, J. A., Patel, R. R., Vasko, M. R., Zhang, J.-M., and Cummins, T. R. (2015) Navβ4 regulates fast resurgent sodium currents and excitability in sensory neurons. *Mol. Pain* **11,** 60 Medline
28. Chen, L., Huang, J., Zhao, P., Persson, A.-K., Dib-Hajj, F. B., Cheng, X., Tan, A., Waxman, S. G., and Dib-Hajj, S. D. (2018) Conditional knockout of $Na_V1.6$ in adult mice ameliorates neuropathic pain. *Sci. Rep.* **8,** 3845 CrossRef Medline
29. Howie, J., Reilly, L., Fraser, N. J., Vlachaki Walker, J. M., Wypijewski, K. J., Ashford, M. L., Calaghan, S. C., McClafferty, H., Tian, L., Shipston, M. J.,

Boguslavskyi, A., Shattock, M. J., and Fuller, W. (2014) Substrate recognition by the cell surface palmitoyl transferase DHHC5. *Proc. Natl. Acad. Sci. U.S.A.* **111,** 17534–17539 CrossRef Medline
30. Lemonidis, K., Sanchez-Perez, M. C., and Chamberlain, L. H. (2015) Identification of a novel sequence motif recognized by the ankyrin repeat domain of zDHHC17/13 *S*-acyltransferases. *J. Biol. Chem.* **290,** 21939–21950 CrossRef Medline
31. Thomas, G. M., Hayashi, T., Chiu, S.-L., Chen, C.-M., and Huganir, R. L. (2012) Palmitoylation by DHHC5/8 targets GRIP1 to dendritic endosomes to regulate AMPA-R trafficking. *Neuron* **73,** 482–496 CrossRef Medline
32. Nadolski, M. J., and Linder, M. E. (2009) Molecular recognition of the palmitoylation substrate Vac8 by its palmitoyltransferase Pfa3. *J. Biol. Chem.* **284,** 17720–17730 CrossRef Medline
33. Huang, K., Sanders, S., Singaraja, R., Orban, P., Cijsouw, T., Arstikaitis, P., Yanai, A., Hayden, M. R., and El-Husseini, A. (2009) Neuronal palmitoyl acyl transferases exhibit distinct substrate specificity. *FASEB J.* **23,** 2605–2615 CrossRef Medline
34. Hou, H., John Peter, A. T., Meiringer, C., Subramanian, K., and Ungermann, C. (2009) Analysis of DHHC acyltransferases implies overlapping substrate specificity and a two-step reaction mechanism. *Traffic* **10,** 1061–1073 CrossRef Medline
35. Plain, F., Congreve, S. D., Yee, R. S. Z., Kennedy, J., Howie, J., Kuo, C.-W., Fraser, N. J., and Fuller, W. (2017) An amphipathic α-helix directs palmitoylation of the large intracellular loop of the sodium/calcium exchanger. *J. Biol. Chem.* **292,** 10745–10752 CrossRef Medline
36. Li, Y., Hu, J., Höfer, K., Wong, A. M., Cooper, J. D., Birnbaum, S. G., Hammer, R. E., and Hofmann, S. L. (2010) DHHC5 interacts with PDZ domain 3 of post-synaptic density-95 (PSD-95) protein and plays a role in learning and memory. *J. Biol. Chem.* **285,** 13022–13031 CrossRef Medline
37. Brigidi, G. S., Santyr, B., Shimell, J., Jovellar, B., and Bamji, S. X. (2015) Activity-regulated trafficking of the palmitoyl-acyl transferase DHHC5. *Nat. Commun.* **6,** 8200 CrossRef Medline
38. Fredericks, G. J., Hoffmann, F. W., Rose, A. H., Osterheld, H. J., Hess, F. M., Mercier, F., and Hoffmann, P. R. (2014) Stable expression and function of the inositol 1, 4, 5-triphosphate receptor requires palmitoylation by a DHHC6/selenoprotein K complex. *Proc. Natl. Acad. Sci. U.S.A.* **111,** 16478–16483 CrossRef Medline
39. Rocks, O., Gerauer, M., Vartak, N., Koch, S., Huang, Z.-P., Pechlivanis, M., Kuhlmann, J., Brunsveld, L., Chandra, A., Ellinger, B., Waldmann, H., and Bastiaens, P. I. (2010) The palmitoylation machinery is a spatially organizing system for peripheral membrane proteins. *Cell* **141,** 458–471 CrossRef Medline
40. Greaves, J., Carmichael, J. A., and Chamberlain, L. H. (2011) The palmitoyl transferase DHHC2 targets a dynamic membrane cycling pathway: regulation by a C-terminal domain. *Mol. Biol. Cell* **22,** 1887–1895 CrossRef Medline
41. Gorleku, O. A., Barns, A.-M., Prescott, G. R., Greaves, J., and Chamberlain, L. H. (2011) Endoplasmic reticulum localization of DHHC palmitoyltransferases *J. Biol. Chem.* **286,** 39573–39584 CrossRef Medline
42. Mill, P., Lee, A. W., Fukata, Y., Tsutsumi, R., Fukata, M., Keighren, M., Porter, R. M., McKie, L., Smyth, I., and Jackson, I. J. (2009) Palmitoylation regulates epidermal homeostasis and hair follicle differentiation. *PLoS Genet.* **5,** e1000748 CrossRef Medline
43. Fernández-Hernando, C., Fukata, M., Bernatchez, P. N., Fukata, Y., Lin, M. I., Bredt, D. S., and Sessa, W. C. (2006) Identification of Golgi-localized acyl transferases that palmitoylate and regulate endothelial nitric oxide synthase. *J. Cell Biol.* **174,** 369–377 CrossRef Medline
44. Herzog, R. I., Cummins, T. R., Ghassemi, F., Dib-Hajj, S. D., and Waxman, S. G. (2003) Distinct repriming and closed-state inactivation kinetics of Nav1.6 and Nav1.7 sodium channels in mouse spinal sensory neurons. *J. Physiol.* **551,** 741–750 CrossRef Medline
45. Cummins, T. R., Rush, A. M., Estacion, M., Dib-Hajj, S. D., and Waxman, S. G. (2009) Voltage-clamp and current-clamp recordings from mammalian DRG neurons. *Nat. Protoc.* **4,** 1103–1112 CrossRef Medline
46. Rush, A. M., Cummins, T. R., and Waxman, S. G. (2007) Multiple sodium channels and their roles in electrogenesis within dorsal root ganglion neurons. *J. Physiol.* **579,** 1–14 CrossRef Medline
47. Maurice, N., Tkatch, T., Meisler, M., Sprunger, L. K., and Surmeier, D. J. (2001) D1/D5 dopamine receptor activation differentially modulates rapidly inactivating and persistent sodium currents in prefrontal cortex pyramidal neurons. *J. Neurosci.* **21,** 2268–2277 CrossRef Medline
48. Khaliq, Z. M., Gouwens, N. W., and Raman, I. M. (2003) The contribution of resurgent sodium current to high-frequency firing in Purkinje neurons: an experimental and modeling study. *J. Neurosci.* **23,** 4899–4912 CrossRef Medline
49. Do, M. T., and Bean, B. P. (2004) Sodium currents in subthalamic nucleus neurons from Nav1.6-null mice. *J. Neurophysiol.* **92,** 726–733 CrossRef Medline
50. Van Wart, A., and Matthews, G. (2006) Impaired firing and cell-specific compensation in neurons lacking Nav1.6 sodium channels. *J. Neurosci.* **26,** 7172–7180 CrossRef Medline
51. Enomoto, A., Han, J. M., Hsiao, C.-F., and Chandler, S. H. (2007) Sodium currents in mesencephalic trigeminal neurons from Nav1.6 null mice. *J. Neurophysiol.* **98,** 710–719 CrossRef Medline
52. Mercer, J. N., Chan, C. S., Tkatch, T., Held, J., and Surmeier, D. J. (2007) Nav1.6 sodium channels are critical to pacemaking and fast spiking in globus pallidus neurons. *J. Neurosci.* **27,** 13552–13566 CrossRef Medline
53. Osorio, N., Cathala, L., Meisler, M. H., Crest, M., Magistretti, J., and Delmas, P. (2010) Persistent Nav1.6 current at axon initial segments tunes spike timing of cerebellar granule cells. *J. Physiol.* **588,** 651–670 CrossRef Medline
54. Royeck, M., Horstmann, M.-T., Remy, S., Reitze, M., Yaari, Y., and Beck, H. (2008) Role of axonal $Na_V1.6$ sodium channels in action potential initiation of CA1 pyramidal neurons. *J. Neurophysiol.* **100,** 2361–2380 CrossRef Medline
55. Smith, M. R., Smith, R. D., Plummer, N. W., Meisler, M. H., and Goldin, A. L. (1998) Functional analysis of the mouse Scn8a sodium channel. *J. Neurosci.* **18,** 6093–6102 CrossRef Medline
56. Raman, I. M., Sprunger, L. K., Meisler, M. H., and Bean, B. P. (1997) Altered subthreshold sodium currents and disrupted firing patterns in Purkinje neurons of Scn8a mutant mice. *Neuron* **19,** 881–891 CrossRef Medline
57. Jarecki, B. W., Piekarz, A. D., Jackson, J. O., 2nd, and Cummins, T. R. (2010) Human voltage-gated sodium channel mutations that cause inherited neuronal and muscle channelopathies increase resurgent sodium currents. *J. Clin. Invest.* **120,** 369–378 CrossRef Medline
58. Landrum, M. J., Lee, J. M., Benson, M., Brown, G., Chao, C., Chitipiralla, S., Gu, B., Hart, J., Hoffman, D., Hoover, J., Jang, W., Katz, K., Ovetsky, M., Riley, G., Sethi, A., *et al.* (2016) ClinVar: public archive of interpretations of clinically relevant variants. *Nucleic Acids Res.* **44,** D862–D868 CrossRef Medline
59. Pankow, S., Bamberger, C., and Yates, J. R., 3rd (2019) A posttranslational modification code for CFTR maturation is altered in cystic fibrosis. *Sci. Signal.* **12,** eaan7984 CrossRef Medline
60. Ho, G. P., Selvakumar, B., Mukai, J., Hester, L. D., Wang, Y., Gogos, J. A., and Snyder, S. H. (2011) *S*-Nitrosylation and *S*-palmitoylation reciprocally regulate synaptic targeting of PSD-95. *Neuron* **71,** 131–141 CrossRef Medline
61. Shipston, M. J. (2014) Ion channel regulation by protein *S*-acylation. *J. Gen. Physiol.* **143,** 659–678 CrossRef Medline
62. Tian, L., Jeffries, O., McClafferty, H., Molyvdas, A., Rowe, I. C., Saleem, F., Chen, L., Greaves, J., Chamberlain, L. H., Knaus, H.-G., Ruth, P., and Shipston, M. J. (2008) Palmitoylation gates phosphorylation-dependent regulation of BK potassium channels. *Proc. Natl. Acad. Sci. U.S.A.* **105,** 21006–21011 CrossRef Medline
63. Summers, D. W., Milbrandt, J., and DiAntonio, A. (2018) Palmitoylation enables MAPK-dependent proteostasis of axon survival factors. *Proc. Natl. Acad. Sci. U.S.A.* **115,** E8746–E8754 CrossRef Medline
64. Woolfrey, K. M., O'Leary, H., Goodell, D. J., Robertson, H. R., Horne, E. A., Coultrap, S. J., Dell'Acqua, M. L., and Bayer, K. U. (2018) CaMKII regulates the depalmitoylation and synaptic removal of the scaffold protein AKAP79/150 to mediate structural long-term depression. *J. Biol. Chem.* **293,** 1551–1567 CrossRef Medline
65. Cummins, T. R., Dib-Hajj, S. D., Black, J. A., and Waxman, S. G. (2000) Sodium channels and the molecular pathophysiology of pain. In *Progress*

in Brain Research, pp. 3–19, Elsevier Science Publishing Co., Inc., New York

66. Herzog, R. I., Liu, C., Waxman, S. G., and Cummins, T. R. (2003) Calmodulin binds to the C terminus of sodium channels Nav1.4 and Nav1.6 and differentially modulates their functional properties. *J. Neurosci.* **23,** 8261–8270 CrossRef Medline
67. Wan, J., Roth, A. F., Bailey, A. O., and Davis, N. G. (2007) Palmitoylated proteins: purification and identification. *Nat. Protoc.* **2,** 1573–1584 CrossRef Medline
68. Pan, Y., and Cummins, T. R. (2020) Distinct functional alterations in SCN8A epilepsy mutant channels. *J. Physiol.* **598,** 381–401 CrossRef Medline